A new look at the infrared properties of $z \sim 5$ galaxies

L. Sommovigo[1⋆], A. Ferrara[1], S. Carniani[1], A. Pallottini[1], P. Dayal[2], E. Pizzati[3], M. Ginolfi[4], V. Markov[1], A. Faisst[4]

[1] *Scuola Normale Superiore, Piazza dei Cavalieri 7, I-56126 Pisa, Italy*
[2] *Kapteyn Astronomical Institute, University of Groningen, 9700 AV Groningen, The Netherlands*
[3] *Leiden Observatory, Leiden University, PO Box 9500, 2300 RA Leiden, The Netherlands*
[4] *European Southern Observatory, Karl-Schwarzschild-Strasse 2, 85748 Garching, Germany*
[5] *IPAC, M/C 314-6, California Institute of Technology, 1200 East California Boulevard, Pasadena, CA 91125, USA*

17 October 2022

ABSTRACT

Recent ALMA large surveys unveiled the presence of significant dust continuum emission in star-forming galaxies at $z > 4$. Unfortunately, such large programs – i.e. ALPINE ($z \sim 5$) and REBELS ($z \sim 7$) – only provide us with a single Far-Infrared (FIR) continuum data point for their individual targets. Therefore, high-z galaxies FIR spectral energy densities (SEDs) remain mostly unconstrained, hinging on an assumption for their dust temperature ($T_{\rm d}$) in the SED fitting procedure. This introduces uncertainties in the inferred dust masses ($M_{\rm d}$), infrared luminosities ($L_{\rm IR}$), and obscured Star Formation Rate (SFR) fraction at $z > 4$. In this work we use a method that allows us to constrain $T_{\rm d}$ with a single band measurement by combining the 158 μm continuum information with the overlying [C II] emission line. We analyse the 21 [C II] and FIR continuum detected $z \sim 5$ galaxies in ALPINE, finding a range of $T_{\rm d} = 25 - 60$ K and $M_{\rm d} = 0.6 - 25.1 \times 10^7$ M$_\odot$. Given the measured stellar masses of ALPINE galaxies, the inferred dust yields are around $M_{\rm d}/M_\star = (0.2 - 8) \times 10^{-3}$, consistent with theoretical dust-production constraints. We find that 8 out of 21 ALPINE galaxies have $L_{\rm IR} \geq 10^{12}$ L$_\odot$, comparable to UltraLuminous IR Galaxies (ULIRGs). Relying on ultraviolet-to-optical SED fitting, the SFR was underestimated by up to 2 orders of magnitude in 4 of these 8 ULIRGs-like galaxies. We conclude that these 4 peculiar sources should be characterised by a two-phase interstellar medium structure with "spatially-segregated" FIR and ultraviolet emitting regions.

Key words: galaxies: high-redshift, infrared: ISM, ISM: structure, methods: analytical – data analysis

1 INTRODUCTION

The Atacama Large Millimeter Array (ALMA) opened a new window on the rest-frame far-infrared (FIR) emission of the first generations of galaxies, dramatically improving our understanding of the dust build-up in the early Universe. Dust grains shape the galaxies Spectral Energy Distributions (SEDs), by absorbing the stellar ultraviolet (UV) and optical radiation, and thermally re-emitting at mid-infrared (MIR, rest-frame $5 - 50$ μm) and far-infrared (rest-frame $50 - 1000$ μm) wavelengths (Draine 1989; Meurer et al. 1999; Calzetti et al. 2000; Weingartner & Draine 2001; Draine 2003). Dust FIR emission is typically modelled as a single-temperature grey-body emission (e.g. Capak et al. 2015; Bouwens et al. 2016; Carniani et al. 2018b; Laporte et al. 2019; Hashimoto et al. 2019; Bakx et al. 2020, 2021, see also Sommovigo et al. 2021), which is characterised mainly by the dust temperature $T_{\rm d}$ and the dust mass $M_{\rm d}$.

Recently, the ALMA large program ALPINE (PI: Le Fèvre, Le Fèvre et al. 2020; Béthermin et al. 2020; Faisst et al. 2020a) provided us with the most abundant sample of FIR continuum detected galaxies at high-z (23 at $z \sim 5$), featuring precise stellar masses $M_\star$ determinations thanks to the wealth of photometric data points available for individual targets. Interestingly, dust-to-stellar mass ratios as large as $M_{\rm d}/M_\star = 0.002 - 0.056$ have been inferred for ALPINE galaxies (Pozzi et al. 2021). Such large dust yields at these early epochs are in tension with theoretical predictions, adding to the so called "dust budget crisis" (e.g. Rowlands et al. 2014, and references therein).

The favoured dust production mechanism at $z \geq 5$ is short lived supernovae (SNe, Todini & Ferrara 2001;

⋆ laura.sommovigo@sns.it

Leśniewska & Michałowski 2019), due to the stringent time constraints imposed by the age of the Universe combined with the young stellar populations in galaxies[1]. However, several works suggest that the dust yield produced in each SN event might be $\lesssim 0.1$ M$_\odot$ after reverse shock processing (Bocchio et al. 2016; Matsuura et al. 2019b; Slavin et al. 2020a; Dayal et al. 2022). This would imply very stringent limits on the expected dust-to-stellar mass ratios, $M_d/M_\star \lesssim 10^{-3}$, in tension with some high-z measurements including the ALPINE ones (see also Tamura et al. 2019; Dayal et al. 2022; Witstok et al. 2022, for higher-z examples).

It is important to stress that these dust masses measurements are heavily dependent on the cold dust temperatures (T_d = 25 K for ALPINE galaxies) *assumed* in the FIR SED-fitting procedure. In fact, most FIR continuum observations at $z > 4$ (typically in ALMA bands 6,7) probe a narrow wavelength range far from the emission peak, where different grey-body curves would deviate the most (e.g. Bouwens et al. 2016; Barisic et al. 2017; Bowler et al. 2018; Hashimoto et al. 2019; Tamura et al. 2019). Therefore, T_d is often fixed in the SED fitting procedure to reach convergence. As a result, all the quantities inferred from fitting, namely M_d, the IR luminosity[2], L_{IR}, and the dust-obscured SFR ($SFR_{IR}/M_\odot yr^{-1} = 10^{-10} L_{IR}/L_\odot$, Kennicutt 1998), are highly uncertain as they depend strongly on the assumed T_d ($SFR_{IR} \propto L_{IR} \propto M_d T_d^6$, see Behrens et al. 2018; Liang et al. 2019; Sommovigo et al. 2020 for a detailed discussion).

Several theoretical works have suggested the presence of warmer dust ($T_d \gtrsim 60$ K) in high-z galaxies (Behrens et al. 2018; Liang et al. 2019; Sommovigo et al. 2020; Pallottini et al. 2022), with temperatures as large as ~ 100 K being reached in the most compact star-forming regions, Giant Molecular Clouds (GMCs, Behrens et al. 2018; Sommovigo et al. 2020). So far, warm dust temperatures $T_d \sim 40-60$ K have been measured in some of the few $z \geq 5$ galaxies (2 of which are included in the ALPINE sample) for which multiple FIR data are available (Faisst et al. 2020a; Bakx et al. 2021; Witstok et al. 2022). Values as large as $T_d > 80$ K have been measured in the only two galaxies detected in multiple ALMA bands at $z \sim 8$ (Laporte et al. 2019; Bakx et al. 2020). Warmer dust temperatures have important implications. They reduce the requirements on M_d to produce the same observed FIR emission (reducing/eliminating the tension with dust production constraints from Supernovae, Behrens et al. 2018; Sommovigo et al. 2020). Warmer T_d values also imply larger obscured SFR fractions (up to $\sim 90\%$ as early as early as $z \sim 7$, e.g. Bakx et al. 2021), despite most of high-z sources observed with ALMA are selected as UV-bright.

Stacked SEDs analysis across a wide redshift range ($z = 0-10$, e.g. Viero et al. 2013; Magnelli et al. 2014; Béthermin et al. 2015; Schreiber et al. 2018; Bouwens et al. 2022; Viero et al. 2022), so far seem to confirm that on average dust is warmer at high-z, further suggesting the existence of a strong correlation between T_d and redshift. A consensus on the $T_d - z$ evolution is yet to be reached, with the largest discrepancies arising at higher-z end, where lesser and more uncertain data are available. In Sommovigo et al. (2022) we proposed a physical model which motivates the increasing $T_d - z$ trend with the decrease of the total gas depletion time $t_{dep} = M_{gas}/SFR$ at high-z, due to the more vigorous cosmological accretion at earlier times. We show that $T_d \propto t_{dep}^{-1/6}$, implying a mild cosmic evolution as $T_d \propto (1+z)^{0.42}$.

The purpose of this paper is to investigate the individual dust and FIR emission properties of the numerous $z \sim 5$ ALPINE galaxies. We are able to do so despite the availability of the single ALMA band-6 measurement thanks to a new method to derive T_d presented in Sommovigo et al. (2021). This method relies on combining the flux at rest-frame 1900 GHz (158 μm) with the overlying [C II] emission-line. In particular, the [C II] luminosity L_{CII} serves as a proxy for the dust mass, breaking the degeneracy between M_d and T_d in the FIR SED-fitting procedure.

With our analysis we can infer the dust masses of ALPINE [C II] and continuum detected sources without the need to rely on an assumption on T_d. We can compare these new results with theoretical dust production constraints at $z \sim 5$. Moreover we can study individual galaxies T_d, L_{IR} and SFR_{IR}, providing a complementary view to stacked FIR SEDs analysis (Béthermin et al. 2020). Deriving ALPINE galaxies T_d also provides a fundamental anchoring to the $T_d - z$ evolution recently extended in the Epoch of Reionization (EoR) thanks to the REBELS galaxies study at $z \sim 7$ (Sommovigo et al. 2022, for details on the REBELS survey see Bouwens et al. 2022). ALPINE continuum-detected galaxies are almost ~ 2 times more numerous than REBELS ones, and span a wider SFR and $M_\star$ range (see Fig. 3), thus constituting a less biased sample with respect to REBELS galaxies (which in turn have the advantage of probing higher-z, where empirical $T_d - z$ relations differ the most). A consistent analysis and thorough comparison of both samples is crucial to solidify our understating of dust properties at high-z.

The paper[3] is organised as follows. In Section 2 we summarize the Sommovigo et al. (2021) method used to compute T_d and its application to ALPINE galaxies. We present our results on the dust temperatures and the $T_d - z$ evolution in Sec. 3. We then discuss the inferred dust masses and compare them with theoretical dust production constraints at $z \sim 5$ in Sec. 4. In Sec. 5 we discuss our estimates on the IR luminosities and obscured SFR fraction, and compare them with the SFR estimates previously obtained based on dust-corrected UV and optical data for ALPINE galaxies. We conclude with a brief summary of our results in Sec. 6.

[1] Asymptotic Giant Branch (AGB) stars are the main dust production sources at low-z. However, at $z \geq 5$ the galaxies ages are typically comparable to the lifetimes of AGB stars (> 150 Myr), making their contribution to dust production likely sub-dominant (e.g. Mancini et al. 2015; Leśniewska & Michałowski 2019; Liu & Hirashita 2019; Burgarella et al. 2020; Nanni et al. 2020; Dayal et al. 2022).

[2] L_{IR} is defined as the integrated continuum luminosity in the rest-frame wavelength range 8 – 1000 μm.

[3] We assume a ΛCDM model with the following cosmological parameters: $\Omega_M = 0.3075$, $\Omega_\Lambda = 1 - \Omega_M$, $\Omega_B = 0.0486$, $h = 0.6774$, and $\sigma_8 = 0.81$. Ω_M, Ω_Λ, Ω_B are the total matter, vacuum, and baryonic densities, in units of the critical density; h is the Hubble constant in units of 100 kms^{-1}, and σ_8 is the late-time fluctuation amplitude parameter (Planck Collaboration et al. 2016).

2 METHOD

In Sommovigo et al. (2021) we proposed a novel method to derive the dust temperature in galaxies relying on a single ALMA measurement, by combining the continuum flux and the [C II] line emission. We briefly summarize the method in the following.

We re-write the equation for the dust continuum flux F_ν observed against the CMB at rest-frame frequency ν = 1900 GHz (F_{1900}) in a more compact form, yielding the following explicit expression for T_d:

$$T_\mathrm{d} = \frac{T_{1900}}{\ln(1+f^{-1})}, \tag{1}$$

where T_{1900} = 91.86 K is the temperature corresponding to the [C II] transition energy at 1900 GHz. The function f is defined as:

$$f = [\exp(T_{1900}/T_\mathrm{CMB}) - 1)]^{-1} + A^{-1}\tilde{F}_{1900}, \tag{2}$$

where T_CMB is the CMB temperature at a given redshift. The non-dimensional continuum flux $\tilde{F}_{1900}$ and the constant A correspond to:

$$\begin{aligned} \tilde{F}_{1900} &= 0.98\times10^{-16}\left(\frac{F_{1900}}{\mathrm{mJy}}\right), \\ A &= 4.33\times10^{-24}\left[\frac{g(z)}{g(6)}\right]\left(\frac{M_\mathrm{d}}{M_\odot}\right), \end{aligned} \tag{3}$$

where $g(z) = (1+z)/d_L^2$ and d_L is the luminosity distance at redshift z.

We use the [C II] luminosity, L_CII, as a proxy for the total gas mass M_g, and thus for M_d given a dust-to-gas ratio D. There is a consensus that D scales linearly with the metallicity, Z, as $D = 1/162\ (Z/Z_\odot)$, with little scatter down to $Z \sim 0.1\ Z_\odot$ (James et al. 2002; Draine & Li 2007; Galliano et al. 2008; Leroy et al. 2011; Rémy-Ruyer et al. 2014). We adopt such scaling for D since we do not expect metallicities $Z \ll 0.1\ Z_\odot$ in relatively evolved and massive ALPINE galaxies (Vanderhoof et al. 2022). We can then write the following expression for M_d:

$$M_\mathrm{d} = D M_\mathrm{g} = D\,\alpha_\mathrm{CII} L_\mathrm{CII}, \tag{4}$$

where α_CII is the [C II]-to-total gas conversion factor.

An analytic expression for α_CII is derived by parametrising in terms of empirical relations such as the Kennicutt–Schmidt relation (Kennicutt 1998, hereafter, KS), and the De Looze relation between L_CII–SFR (De Looze et al. 2014), which has been shown to be valid for ALPINE galaxies by Schaerer et al. (2020). This yields

$$\alpha_\mathrm{CII} = 32.47\ \frac{y^2}{\kappa_\mathrm{s}^{5/7}}\ \Sigma_\mathrm{SFR}^{-0.29}\ \frac{M_\odot}{L_\odot}, \tag{5}$$

where Σ_SFR is the SFR surface density[4] and κ_s is the "burstiness parameter" which quantifies deviations from the KS relation, $\kappa_s = \Sigma_\mathrm{SFR}/(10^{-12}\ \Sigma_\mathrm{gas}^{1.4})$ ($\kappa_\mathrm{s} > 1$ for starbursts and $\kappa_\mathrm{s} < 1$ for quiescent galaxies; see Ferrara et al. 2019; Pallottini et al. 2019; Vallini et al. 2020). The [C II]-to-UV emission size ratio, $y = r_\mathrm{CII}/r_\star$, is introduced as there is growing evidence that at $z > 4$ [C II] emission extends further than star-forming regions ($1.5 \lesssim y \lesssim 3$ at $z > 4$, see Carniani et al. 2017, 2018a, 2020; Matthee et al. 2017, 2019; Fujimoto et al. 2019, 2020; Rybak et al. 2019; Ginolfi et al. 2020).

The method described here has been tested on a sample of 19 local galaxies and 10 galaxies at $z \gtrsim 4$ (Sommovigo et al. 2021, 2022; Bakx et al. 2021). For all these galaxies[5] multiple data points in the FIR SED are available, allowing us to compare our inferred dust temperatures with robust T_d estimates obtained with traditional SED fitting. We recovered consistent dust temperatures within ±30% uncertainty spanning the redshift range $z = 0 - 8.31$ as well as the temperature range 20 K $\lesssim T_\mathrm{d} \lesssim$ 100 K. We also tested our method on simulations, applying it to the $z \sim 6.7$ galaxy Zinnia (a.k.a. serra05:s46:h0643) from the SERRA simulation suite (Pallottini et al. 2022). Also in this case, we recover T_d in agreement with single-temperature grey body SED fitting performed at the frequencies corresponding to ALMA bands 6, 7, and 8.

2.1 Application to ALPINE galaxies

We aim at deriving the dust masses and temperatures $(M_\mathrm{d}, T_\mathrm{d})$ of the 21 ALPINE galaxies detected both in [C II] and in continuum[6] at rest-frame 1900 GHz. The physical properties needed for the application of our method are all constrained by observations[7] (see Tab. 1 for all galaxies measured properties used in this work), with the exception of (κ_s, Z).

The burstiness parameter κ_s and metallicity Z of ALPINE galaxies are unknown, thus a broad range of values is assumed for each quantity. Values as large as $\kappa_\mathrm{s} \simeq 100$ have been observed in star-forming galaxies both locally and at intermediate-redshift (see e.g. Daddi et al. 2010). By applying the [C II]-emission model given in Ferrara et al. (2019) on 12 bright UV-selected galaxies at $z = 6-9$, Vallini et al. (2020, 2021) found that κ_s values spanning the range $\sim 3-80$. Based on these findings, for ALPINE galaxies we choose a random uniform distribution in the range $1 \lesssim \kappa_\mathrm{s} \lesssim 80$.

For the metallicity, we assume a uniform random distribution of values in the range $0.3 - 1\ Z_\odot$. This is based on numerical simulations results for galaxies at $z \lesssim 6$ with similar stellar masses as ALPINE galaxies $10^9 < M_\star/M_\odot < 10^{11}$

[4] Σ_SFR is in units of $[\mathrm{M_\odot yr^{-1} kpc^{-2}}]$.

[5] The 10 high-z galaxies test sample includes 4 sources from the Capak et al. (2015) sample, followed-up in multiple ALMA bands by Faisst et al. (2020b). Two of these 4 sources (HZ4 and HZ6) are also included in the ALPINE sample, see the discussion in Sec. 3.

[6] We do not consider 2 out of the 23 [C II] and continuum detected ALPINE sources, as their UV sizes, $r_\star$, and/or stellar masses $M_\star$ were not constrained.

[7] Measurements of r_CII are provided by Fujimoto et al. (2020) for all ALPINE sources except the galaxy VC 5101209780, which was left out due to its signal-to-noise ratio SNR < 5. For this source, we measure the [C II] radius in this work. We retrieve the ALMA continuum-subtracted, integrated [C II] line map (from the ALPINE website, http://alpine.ipac.caltech.edu) and exploit the CASA task imfit software. We fit the [C II] map with a 2D elliptical Gaussian model, and measure the beam-deconvolved FWHMs in arcseconds. We then infer r_CII from the mean of the beam-deconvolved major and minor axes. The result is given in Tab. 1. We have checked that this procedure gives r_CII estimates consistent to the ones provided by Fujimoto et al. (2020), where available.

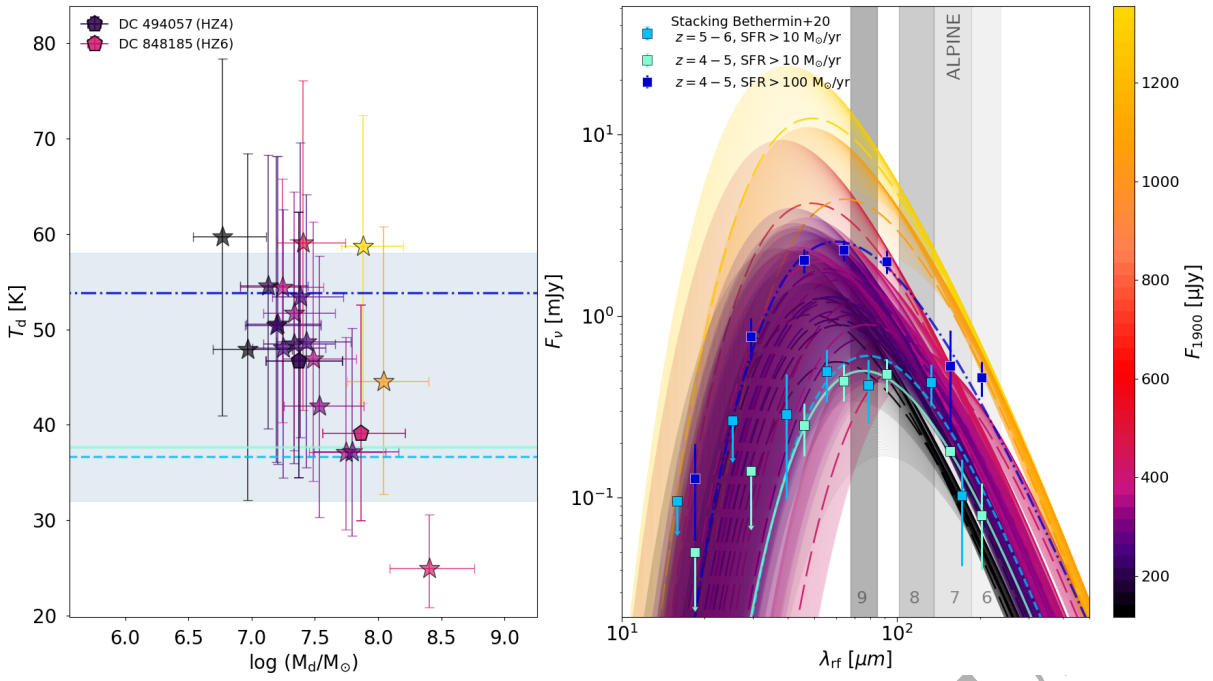

Figure 1. Left Panel: Dust temperature T_d and dust mass M_d derived for the ALPINE galaxies detected both in [C II] and FIR continuum. The points are colour-coded according to their observed continuum flux F_{1900}. The two sources HZ4 and HZ6 for which multiple continuum data (and thus T_d, M_d estimates) are highlighted. The horizontal lines and blue shaded area show the T_d values and associated uncertainties, obtained by fitting the stacked data shown in the right panel with the same colors. **Right panel**: FIR SEDs obtained using the (T_d, M_d) and associated uncertainty derived for ALPINE galaxies (shown in the left panel). The lines are colour-coded as in the left panel. The blue and green points show the stacked data by Béthermin et al. (2020) at $z = 4-6$. The three different colours correspond to different cuts in the redshift and SFR of the stacked sources: $z = 4-5$ and SFR > 10 $M_\odot$/yr (green), $z = 4-5$ and SFR > 100 $M_\odot$/yr (light blue), and $z = 5-6$ and SFR > 10 $M_\odot$/yr (darkblue). The grey shaded area marks the FIR wavelengths traced by ALMA bands 6 – 9 (ALMA band 7 is the one used in the ALPINE survey).

(Ma et al. 2016; Torrey et al. 2019), and several observational studies which analyse FIR lines (such as [N II], [N III], [C II], [O II] and [O III]) to infer Z in galaxies up to $z \sim 6-8$ (Pereira-Santaella et al. 2017; Hashimoto et al. 2019; De Breuck et al. 2019; Tamura et al. 2019; Vallini et al. 2020; Bakx et al. 2020; Jones et al. 2020; Ucci et al. 2021). In particular, Vanderhoof et al. (2022) infer an average metallicity $Z/Z_\odot \sim 0.5$ for 10 ALPINE galaxies based on their measured [O II]-to-CII ratios. Better constraints on galaxies metallicities out to $z \sim 10$ will be available soon thanks to the James Webb Space Telescope (JWST) spectroscopic observations of rest-frame optical nebular lines (such as Hβ , Hα , [N II], [O II] and [O III], Maiolino & Mannucci 2019; Chevallard et al. 2019; Curti et al. 2022).

We can now compute the [C II]-to-total gas conversion coefficient α_{CII} for the ALPINE sources using eq. 5. We find on average $\langle\alpha_{CII}\rangle = 8^{+3}_{-5}$, which is consistent with our previous findings for $z > 4$ galaxies (Sommovigo et al. 2021, 2022). Note that in local sources we find much larger conversion factors, up to $\alpha_{CII} \lesssim 10^3$. This might suggest that for a given [C II] luminosity high-z galaxies have a lower gas content (or that for a given gas content they have higher [C II] emission; for a detailed discussion see e.g. Ferrara et al. 2019). For the comparison with the empirical *molecular*-to-[C II] conversion factor $\alpha_{CII,mol} = \Sigma_{H_2}/\Sigma_{CII} = 31^{+31}_{-16}$ derived in Zanella et al. (2018) we refer to Sommovigo et al. 2022 (Sec. 3).

We can now estimate M_d and T_d for all the targets, and thus L_{IR} and SFR_{IR}. The results are summarised in Fig. 1, reported in Tab. 2, and discussed in detail in the following Sections.

3 DUST TEMPERATURES

We find the dust temperatures of ALPINE galaxies to lay within the wide range 25−60 K, with an average value around $\langle T_d \rangle = 48 \pm 8$ K. The relative error associated to the individual sources T_d is around $\Delta T_d/T_d \sim 30\%$, with the dominant contributions to this uncertainty coming from the metallicity and burstiness parameter. Albeit large, this $\Delta T_d/T_d$ is comparable to that obtained from traditional SED fitting at similarly high-z when multiple FIR data are available (see e.g. Harikane et al. 2020; Hashimoto et al. 2019; Bowler et al. 2018). Among the ALPINE targets there are two galaxies, DC 494057 and DC 848185 (HZ4 and HZ6 from Capak et al. 2015), for which ALMA bands 6,7, and 8 observations are available thanks to dedicated follow-up observations by Faisst et al. (2020b). For both sources, the T_d values derived with our method are consistent with traditional SED fitting results within less than $\lesssim 20\%$ uncertainty.

In Béthermin et al. (2020) the authors attempt at constraining the average T_d of ALPINE galaxies by fitting the stacked, single-dish FIR data from a photometric sample similar to ALPINE at $z = 4-6$. The stacked targets in Béthermin et al. (2020) are selected to resemble ALPINE

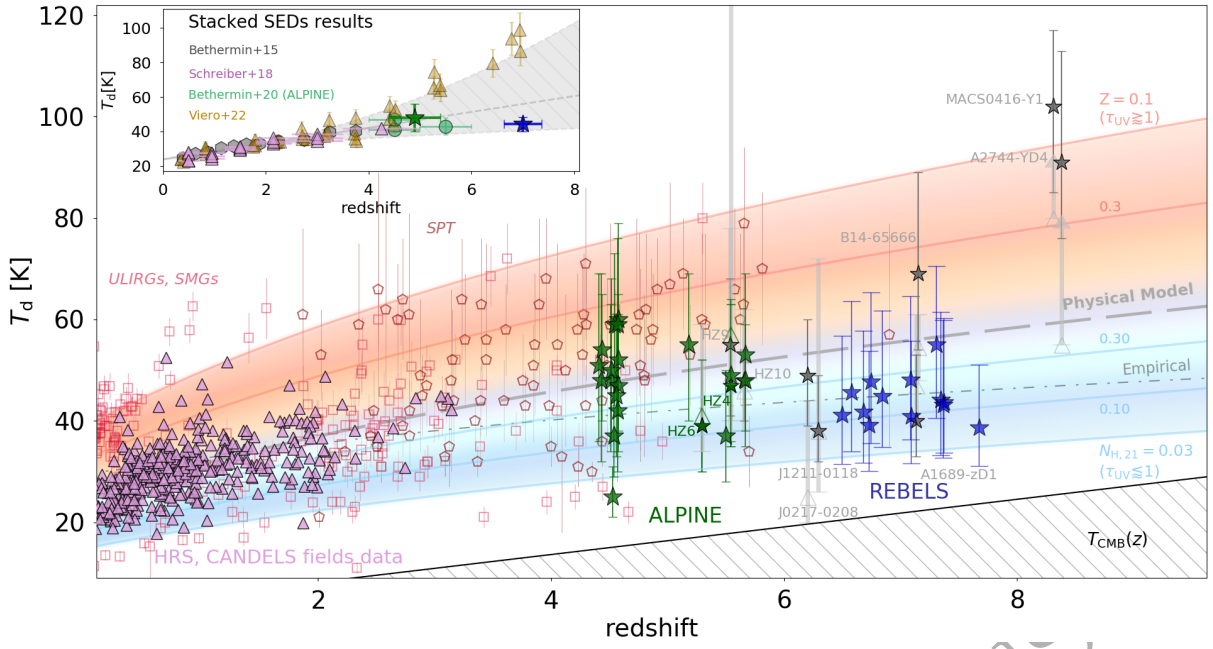

Figure 2. Main panel: Dust temperature T_d as a function of redshift for star-forming galaxies in the range $z = 0-8$ *(updated version of Fig. 2 in Sommovigo et al. 2022)*. The purple triangles represent the UV-to-IR normal star-forming galaxies detected in the HRS and CANDELS fields studied in Schreiber et al. (2018), which have comparable $M_\star$ to ALPINE and REBELS galaxies ($10^{9.5} \leq M_\star/M_\odot \leq 10^{11.5}$). The maroon and red empty symbols represent respectively the sub-mm galaxies observed at $z \lesssim 2$ (Yang et al. 2007; Magdis et al. 2014; Huang et al. 2014; Chapman et al. 2005; Clements et al. 2018) and at $z = 2-4$ (SPT sample, Reuter et al. 2020). The grey points show the individual UV-selected galaxies at $z > 5$ for which T_d estimates are available thanks to multiple FIR continuum observations. Both the T_d values obtained with our method and with traditional SED fitting are shown (respectively as stars and triangles; we note that in all cases the two estimates are consistent within $1-\sigma$, for further details see Sommovigo et al. 2022). Finally, in green and blue we show the results obtained with our method for individual ALPINE and REBELS galaxies, respectively. The coloured region shows the T_d-redshift evolution that we derive analytically in Sommovigo et al. 2022 (for an increasing effective UV optical depth τ_{UV} from blue to red). We find that on average T_d raises with redshift due to the decreasing gas depletion time $t_{dep} = M_g/SFR$ at higher-z, as $T_d(z) \propto t_{dep}^{-1/6}$. This dependence is shown by the grey dashed line for $t_{dep} \propto (1+z)^{-2.5}$ – derived from numerical simulations – implying $T_d \propto (1+z)^{0.4}$. For comparison, we also show the $T_d - z$ relation we would predict based on the empirical evolution $t_{dep,H_2} \propto (1+z)^{-1.5}$ inferred by Tacconi et al. 2020 for main-sequence galaxies (grey dotted-dashed line). **Inset panel:** T_d values obtained from stacked SEDs fitting in the redshift range $0 \lesssim z \lesssim 8$ (grey, purple, green and yellow points, from Béthermin et al. 2015; Schreiber et al. 2018; Béthermin et al. 2020; Viero et al. 2022, respectively). The grey hatched area shows the different $T_d - z$ trends empirically derived in these works, with the lower (upper) bound being set by Liang et al. 2019 (Viero et al. 2022). The linear $T_d - z$ relation derived by Schreiber et al. 2018 is also shown. The green (blue) star corresponds to the average temperature derived here for ALPINE (REBELS) galaxies.

galaxies in stellar mass, $M_\star > 3\times10^{10}$ $M_\odot$, and star formation rate, SFR> 10 $M_\odot$/yr (derived from optical and near-infrared SED fitting). They are divided in two redshift bins at $z = 4-5$ (5749 sources) and $z = 5-6$ (1883 sources). The comparison of these stacked data with the individual ALPINE galaxies SEDs derived with our method is shown in Fig. 1. We find that most (all but 3) of the individual ALPINE galaxies FIR SEDs are bracketed by the stacked SEDs. In fact, by fitting the stacked SEDs with the same dust model adopted for the individual galaxies[8] we find $T_d = 37-54$ K, consistent (albeit slightly lower) with the range of dust temperatures obtained with our method. This consistency between SEDs of individual continuum-detected sources and stacked data is encouraging as stacking is widely used to extend star-forming galaxies IR emission studies out to $z \gtrsim 4$ (see e.g. Béthermin et al. 2015; Schreiber et al. 2018; Béthermin et al. 2020; Viero et al. 2022).

3.1 Cosmic T_d evolution

Recently, several works have alluded to the presence of a cosmic evolution of the dust temperature in star-forming galaxies (Magdis et al. 2012; Magnelli et al. 2013; Viero et al. 2013; Béthermin et al. 2015; Schreiber et al. 2018; Faisst et al. 2020a; Liang et al. 2019; Bouwens et al. 2020; Reuter et al. 2020). In most of these studies, the average T_d at a given epoch is derived by fitting stacked data, including observations at wavelengths shorter than $\lambda \lesssim 350$ μm from the Herschel space observatory. Herschel was the only instrument probing these MIR-to-FIR wavelengths, which are crucial to obtain stringent constraints on T_d. However, Herschel cannot detect individual galaxies at $z \gtrsim 2$ because of confusion (e.g. Magdis et al. 2012; Magnelli et al. 2014), thus requiring to rely on stacking at higher-z.

Interestingly, different works find discrepant results (see

[8] We consider Milky Way-like dust, for which standard values for the dust opacity $\kappa_\nu = \kappa_\star(\nu/\nu_\star)^{\beta_d}$ are $(\kappa_\star, \nu_\star, \beta_d) = (10.41\ cm^2g^{-1}, 1900\,GHz, 2.03)$, from Weingartner & Draine 2001; Draine 2003.

inset panel in Fig. 2). Some works suggest a linearly increasing $T_d - z$ trend based on stacked SEDs fitting results in the redshift range $z = 0-5$ (Schreiber et al. 2018), coupled with a few individual detections at $z \gtrsim 5$ (Bouwens et al. 2020). Other works predict a much milder evolution (Magnelli et al. 2013; Viero et al. 2013; Reuter et al. 2020); in particular Liang et al. (2019) find a substantial flattening in the increase of T_d at $z \gtrsim 4$ based on SED fitting procedure applied to the FIRE simulations at $z = 2-6$. This flattening in the $T_d - z$ evolution is consistent with individual galaxies peak dust temperatures ($T_{peak} \sim 2.9 \times 10^3 (\lambda_{peak}/\mu m)^{-1}$) measured at $z \sim 4-5$ by Faisst et al. (2020b). However, T_{peak} can significantly differ from T_d depending on the adopted SED fitting function. In fact, Faisst et al. (2020b) finds $T_d > T_{peak}$ ($\delta T_d \sim 13$ K on average), consistently with our derivation (see Sec. 3). It is worth mentioning that the only two $z \sim 8$ ALMA-detected sources host hot dust with temperatures $T_d = 90-100$ K (see also Behrens et al. 2018; Bakx et al. 2020; Laporte et al. 2019), possibly questioning such scenario. We stress that for these 2 galaxies we are able to uniquely derive T_d by combining the [C II] luminosity information with the rest-frame 88 μm continuum flux[9]. These hot dust temperatures at $z \sim 8$ are consistent with the results by Viero et al. (2022), where they exploit the recently released COSMOS2020 catalogue (Weaver et al. 2022) to extend stacked SEDs studies up to unprecedentedly high-z ($z \sim 10$). The reliability of these stacking results at $z \gg 4$ is somewhat uncertain, as individuating low-z interlopers and/or correcting for the bias towards the brightest sources becomes more challenging (see the discussion in Viero et al. 2022). We caution that Viero et al. (2022) find a nearly constant number of very massive sources (~ 60 at $M_\star \gtrsim 10^{11}$ M$_\odot$) in their stacked bins at $z = 3.5-4$ and $z = 8-10$, which is in contrast with the predictions from the stellar mass function. In fact, extrapolating abundance matching results (Behroozi et al. 2019) and observations (Song et al. 2016) at $z \leq 8$ and $M_\star \leq 3\times10^{10}$ M$_\odot$, we would expect a > 2 odm drop in the number density of $M_\star \gtrsim 10^{11}$ M$_\odot$ sources from $z = 4$ to $z > 8$. Semi-analytical models such as DELPHI (Dayal et al. 2022) agree with this prediction, with a steep drop in the number density (7 odm) at the high-mass end ($M_\star = 4 \times 10^{10}$ M$_\odot$) from $z = 4$ to $z = 10$. Upcoming JWST observations will allow us to extend the census of massive systems at $z > 8$, testing these predictions (Castellano et al. 2022; Naidu et al. 2022; Labbe et al. 2022).

Thanks to our method, for the first time we constrain T_d in a large number of sources (40) at $z \gtrsim 4$, thus adding fundamental and highly complementary information from individual galaxies analysis to stacked SED results. At $z = 4.9$, the mean redshift of [C II] and continuum detected ALPINE galaxies, we find an average $\langle T_d \rangle = 48 \pm 8$ K, whereas $\langle T_d \rangle = 44 \pm 4$ K for the 13 [C II] and continuum-detected REBELS galaxies at $z \sim 7$ (Bouwens et al. 2022; Inami et al. 2022). We note that this value for REBELS galaxies $\langle T_d \rangle$ is slightly lower than the one reported in Sommovigo et al. (2022) ($T_d = 47 \pm 7$ K). We have updated the stellar masses of REBELS galaxies to the latest values by Topping et al. (2022), obtained by assuming a non-parametric star-formation history (SFH, instead of constant SF). A non-parametric SFH results in an increase in $M_\star$ up to one order of magnitude for galaxies with large specific SFR[10]. Larger $M_\star$ imply slightly larger dust M_d and lower T_d to reproduce the same observed F_{1900}.

The comparable average T_d in ALPINE and REBELS galaxies, whose main difference is the redshift of the sources[11], questions the validity of the simple, linearly increasing $T_d - z$ trend suggested by Schreiber et al. (2018); Bouwens et al. (2020) (predicting an increase from $T_d \sim 46$ K at $z = 4.9$ to 56 K at $z = 7$). On the other hand, the flattening in the $T_d - z$ trend at $z > 4$ inferred by Magnelli et al. (2013); Liang et al. (2019) seems too extreme (they predict colder temperatures, $T_d \sim 37$ K at $z = 4.9$ and $T_d \sim 39$ K at $z = 7$). The largest discrepancy is with the preliminary results by Viero et al. (2022), whose best fitting $T_d - z$ relation features a sharp increase in T_d at $z \gtrsim 5$ reaching $T_d \sim 87$ K at $z = 7$ (almost $\times 2$ higher than the average dust temperature we find in REBELS galaxies at the same redshift). A possible caveat is that both ALPINE and REBELS sources are UV-selected as the brightest sources at their respective redshift, thus constituting a biased sample, possibly skewed toward colder dust temperatures (e.g. Chen et al. 2022b). JWST will allow us to probe relatively UV-faint galaxies also at $z \geq 5$; by following-up JWST observations with ALMA, we will investigate also UV-faint high-z galaxies dust properties, possibly reducing the current observational bias.

In Sommovigo et al. (2022) we produced a model aimed at physically motivating the cosmic evolution of the dust temperature. Assuming FIR and UV emission to be co-spatial, from simple conservation of energy argument, we show that T_d anti-correlates with the *total* gas depletion time as $T_d \propto t_{dep}^{-1/6}$. The increase of the cosmological accretion rate at early times (Fakhouri et al. 2010; Dekel & Krumholz 2013; Correa et al. 2015), results in high-z galaxies being more efficiently star forming, thus implying shorter t_{dep} at high-z. As a result, we predict mild increase of T_d with redshift as:

$$T_d \propto t_{dep}^{-1/6} \approx (1+z)^{0.42}. \quad (6)$$

where the adopted $t_{dep} - z$ evolution ($t_{dep} \propto (1+z)^{-2.5}$) is taken from numerical simulations (Fakhouri et al. 2010; Dekel & Krumholz 2013; Correa et al. 2015) due to the lack of observational constraints on the atomic gas content of high-z galaxies. The *molecular* gas depletion time, $t_{dep,H_2} = M_{H_2}/SFR$, has been indirectly studied up to $z \sim 6$ relying on CO and dust observations (e.g. Walter et al. 2020; Tacconi et al. 2020; Dessauges-Zavadsky et al. 2020). For main-sequence galaxies, different works consistently infer an evolution of t_{dep,H_2} with redshift around $t_{dep,H_2} \propto (1+z)^{-1.5}$ (Tacconi et al. 2020). Adopting such empirical $t_{dep,H_2}(z)$ relation, would imply an milder - but still significant- cosmic T_d evolution $T_d \propto (1+z)^{0.25}$. This is also shown in Fig. 2.

On top of the $T_d - z$ trend, Sommovigo et al. (2022)

[9] From traditional SED fitting only a lower limit on $T_d > 50, 80$ K is obtained (Bakx et al. 2020; Laporte et al. 2019), see Appendix B in (Sommovigo et al. 2022).

[10] This increase in $M_\star$ is due to the presence of a significant old stellar population that is out-shined by the recent star formation (SF) burst

[11] REBELS galaxies stellar masses and SFRs are similar -albeit spanning a narrower range- to that of ALPINE galaxies, being $9 \lesssim \log(M_\star/M_\odot) \lesssim 10$ and $20 \lesssim SFR/M_\odot yr^{-1} \lesssim 200$.

showed that the scatter in the measured T_d values at a given redshift can be explained by the variation of a few key individual galaxies properties, namely the optical depth τ_{UV}, metallicity and column density $N_H \sim 10^{21} \tau_{UV}/Z$ cm^{-2}. The results derived in this paper for individual ALPINE galaxies are consistent with the predictions from our physical model, as shown in Fig. 2. Due to the different redshifts of the ALPINE and REBELS samples, we expected a minor mean temperature variation $|\langle T_{d,REB}\rangle - \langle T_{d,ALP}\rangle| / \langle T_{d,ALP}\rangle \sim 14\%$. However, such variation is comparable to the $1-\sigma$ error associated to $\langle T_d \rangle$ in the two samples.

The slightly warmer T_d of ALPINE galaxies with respect to REBELS galaxies could be explained by larger UV optical depths, implying a more efficient dust heating. This prediction is qualitatively confirmed by the measured average UV slopes $\langle \beta_{UV} \rangle$ for the two samples. In fact, $\langle \beta_{UV} \rangle$ is redder in ALPINE galaxies (-1.4 ± 0.5) than in REBELS galaxies (-1.8 ± 0.3), implying a larger dust-obscuration (as a reference, we remind the intrinsic UV slope[12] amounts to $\beta_{int} = -2.406$, Ferrara et al. 2022). Our prediction of warmer dust temperatures in more UV-obscured systems is also confirmed by the comparison with sub-millimeter galaxies studies at $z \lesssim 6$ (see Fig. 2). In fact, on average sub-mm galaxies host warmer dust than UV-trasparent galaxies (see also Faisst et al. 2020b), reaching values around $T_d \sim 40$ K in the local Universe (Yang et al. 2007; Magdis et al. 2014; Huang et al. 2014; Chapman et al. 2005; Clements et al. 2018), and $T_d \sim 60$ K at $z \sim 5$ (Reuter et al. 2020)[13].

4 DUST MASSES

We derive the dust masses for our sample of the ALPINE galaxies finding them to vary within the range $6.77 < \log(M_d/M_\odot) < 8.41$, with the average value being $\langle \log(M_d/M_\odot) \rangle = 7.47 \pm 0.37$. This value is a factor ~ 7 lower than the values reported in Pozzi et al. (2021) for these same galaxies. Pozzi et al. (2021) *assume* a very cold dust temperature of 25 K, to derive the dust masses from the continuum fluxes F_{1900}. They state that this value (which is close to $T_{CMB}(z = 6)$) should correspond to the mass-weighted dust temperature of typical $z \sim 6$ galaxies. However, by analysing an average simulated galaxy at $z \sim 6$ from the SERRA simulation suite (Pallottini et al. 2019, 2022), in Sommovigo et al. (2021) we found that the mass-weighted dust temperature and T_d derived from fitting the simulated spectra (using mock continuum observations in ALMA band 6,7, and 8 or our method) actually correspond, and are $\gg T_{CMB}$ ($T_d \sim 60$ K, see also Pallottini et al. 2022 for an extended discussion). The temperatures that we infer for ALPINE galaxies are similarly warm, $T_d \sim 48$ K, with a single exception represented by the galaxy VC 5180966608 for which we infer $T_d = 25$ K. This cold dust results from the peculiar, and likely unreliable, [C II]-to-UV size ratio measured for this galaxy. In fact, from eq. 4-5 it follows that $M_d \propto y^2 = (r_{CII}/r_\star)^2$, resulting in a much larger dust mass for VC 5180966608, whose $y = 10$, with respect to the other galaxies in the ALPINE sample, where on average $\langle y \rangle \sim 3$. This massive dust content ($\log(M_d/M_\odot) = 8.41$), coupled with a relatively low continuum flux ($F_{1900} = 462$ μJy), results in the exceptionally cold dust temperature derived for this galaxy. However, the [C II] size of VC 5180966608 is flagged as unreliable by Fujimoto et al. (2020) due to its complicated morphology. In fact, in the latest analysis by Romano et al. (2021) VC 5180966608 is classified as a merger; treating it as a single source might have lead us to misinterpreting its properties. Upcoming deeper ALMA [C II] observations and higher resolution FIR continuum data from the CRISTAL

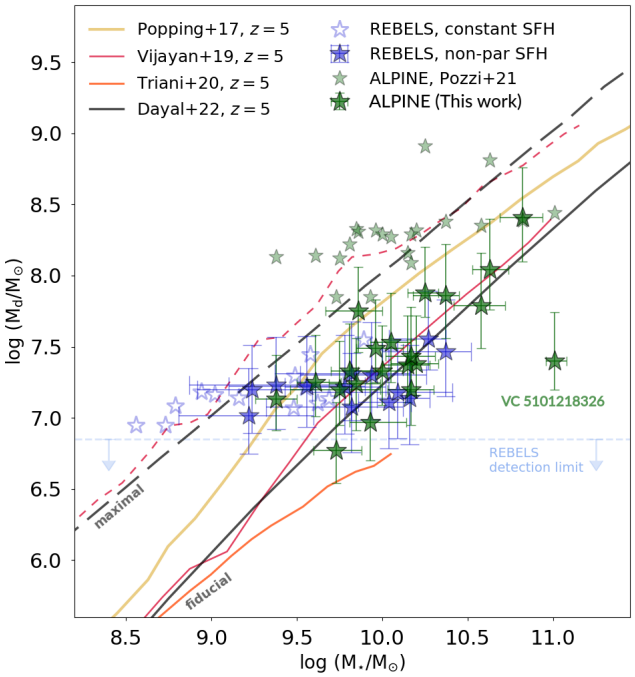

Figure 3. Dust mass M_d as a function of stellar mass $M_\star$. The solid green stars show the M_d values that we derive for ALPINE galaxies, whereas the transparent ones were obtained by Pozzi et al. (2021) assuming $T_d = 25$ K. The blue stars (empty stars) represent REBELS galaxies, where $M_\star$ is inferred assuming a non-parametric SFH (constant SF, Topping et al. 2022). The solid lines show the fiducial predictions at $z \sim 5$ from semi-analytical models such as DELPHI (black, Dayal et al. 2014, 2022), Santa Cruz (yellow, Popping et al. 2017), DUSTY SAGE (orange, Triani et al. 2020), and L-GALAXIES (red, Vijayan et al. 2019). The dashed lines show the maximal predictions of the corresponding models, assuming no dust destruction or ejection, and saturated grain growth. We find that all but one ALPINE galaxies are consistent with theoretical predictions. This is not true for higher-z REBELS galaxies (particularly under the assumption of constant SF), whose $M_d - M_\star$ relation appears flat; possible explanations are discussed in the text (see also Dayal et al. 2022). The dashed blue line shows the M_d detection threshold for the REBELS program assuming a non-detection flux limit of 42 μJy and $T_d = 48$ K.

[12] The quoted intrinsic UV slope is obtained from STARBUST99 (Leitherer et al. 1999), assuming continuous star formation, Salpeter IMF 1 – 100 $M_\odot$, metallicity $Z = 1/3$ $Z_\odot$, and stellar age 150 Myr.

[13] We caution that the SED-fitting procedure used in Reuter et al. (2020) for SPT galaxies is different with respect to the one adopted here, which assumes an optically thin grey-body emission. Nevertheless, when testing our method on the only SPT galaxy with available metallicity measurements (SPT 0418-47), we found consistent results with Reuter et al. (2020) within $1-\sigma$ (Sommovigo et al. 2021).

large program (PI: Herrera-Camus) will allow us to further investigate this hypothesis.

The lower dust masses that we infer for ALPINE galaxies have important implications in terms of the comparison with theoretical dust production constraints at $z \sim 5$. We discuss this in detail in the following Section.

4.1 Dust production at $z \gtrsim 5$

We begin by computing the dust yield y_d per SN which would be required to produce the dust masses derived in this work for ALPINE galaxies. This is $y_d/M_\odot = M_d/(\nu_{SN} M_\star)$, where $\nu_{SN} = (53\ M_\odot)^{-1}$ is the rate of SNe per solar mass of stars formed assuming a Salpeter $1-100\ M_\odot$ IMF (Ferrara & Tolstoy 2000). We find that on average $\langle y_d \rangle = 0.15 \pm 0.09\ M_\odot$, which is consistent with the SN dust production constraints by Leśniewska & Michałowski (2019). However, other works suggest that the dust yield spared in a SN blast is as low as $\lesssim 0.1 M_\odot$ (Bocchio et al. 2016; Matsuura et al. 2019a; Slavin et al. 2020b).

In order to investigate dust production further, in Fig.3 we compare the dust-to-stellar mass relation that we find for ALPINE galaxies with predictions from semi-analytical dust production models at $z \sim 5$. We include the DELPHI model (Dayal et al. 2014, 2022), the Santa Cruz model (Popping et al. 2017), DUSTY SAGE (Triani et al. 2020), and L-GALAXIES (Vijayan et al. 2019), which (mostly) cover the ALPINE stellar mass range $M_\star = 10^9 - 10^{11}\ M_\odot$. All these models include varying prescriptions for gas cooling, star formation, SN feedback, chemical enrichment and key dust processes, namely dust formation, astration, destruction in SNe shocks, ejection in outflows, and grain growth. The DELPHI model does not include the contribution of AGB stars to dust production, which is likely sub-dominant due to the long timescales required for such dust production mechanism ($\gtrsim 150$ Myr) and the conflicting young stellar ages of $z \gtrsim 5$ galaxies (e.g. Leśniewska & Michałowski 2019; Liu & Hirashita 2019; Nanni et al. 2020; Dayal et al. 2022).

Our results are consistent (within $1-\sigma$) with DELPHI and L-GALAXIES theoretical predictions, with the Santa Cruz model favouring slightly larger dust masses (for nearly 50% of the sample). The slope of the $M_d - M_\star$ relation is consistent with our results in all the four models. therefore, it is not necessary to invoke unphysical scenarios with no dust destruction or ejection, and saturated grain growth. Moreover, dust production from SNe described by the DELPHI model is able to reproduce the inferred dust masses for most of the ALPINE galaxies (72% within $1-\sigma$ and the remaining ones within $1.5-\sigma$), confirming that the contribution to dust production from AGB stars in ALPINE galaxies is subdominant. The most discrepant galaxy is VC 5101218326, for which we predict a surprisingly low dust mass $M_d = 10^{7.4}\ M_\odot$, roughly one order of magnitude below theoretical predictions given the galaxy large stellar mass $M_\star = 10^{11}\ M_\odot$. This source is one of the two most peculiar sources in the ALPINE sample in terms of its dust properties and will be discussed in detail in the following Section.

Finally, we compare our results for the dust-to-stellar mass ratios in ALPINE galaxies, with the ones obtained for the REBELS sources with the same method (Sommovigo et al. 2022; Dayal et al. 2022). By using the larger $M_\star$ values derived for REBELS galaxies assuming a non-parametric SFH instead of constant SF (Topping et al. 2022), the discrepancy with theoretical models is reduced (none of the sources exceeds the maximal dust production constraints). In fact, for less massive objects ($\log(M_\star/M_\odot) \leq 10^{9.5}$) the increase in $M_\star$ can be as large as 1 dex, while M_d is marginally affected (30% variation). However, differently from ALPINE galaxies, in the higher-z REBELS sample we do not recover the $M_d - M_\star$ correlation predicted by analytical models (independently from the assumed SFH). In fact, REBELS galaxies dust masses appear to be independent from their stellar masses. ALPINE galaxies are more massive than REBELS objects, and overall cover a larger range of $M_\star$ values. This might indicate that flatness of the $M_d - M_\star$ trend found for REBELS galaxies largely depends on an observational bias due the limited range of stellar masses probed by this survey[14]. Further ALMA observations probing the dust content of galaxies in a wider stellar mass range both at $z = 7$ and $z = 5$, will confirm whether we are witnessing an evolution in the dust-to-stellar mass relation between these two epochs. This could imply that also the mass-metallicity relation (to whom our dust-to-stellar mass relation is directly connected as we assume $D \propto Z$) breaks down at $z > 6$.

5 IR LUMINOSITIES AND TOTAL SFR

We compute the IR luminosities using the following relation (Ferrara et al. 2022; Sommovigo et al. 2022):

$$L_{IR} = \left(\frac{M_d}{M_\odot}\right)\left(\frac{T_d}{8.5\,K}\right)^{6.03} L_\odot. \quad (7)$$

valid for the Milky Way (MW) dust model adopted here. We find that ALPINE galaxies IR luminosities vary in the range $1.7\times10^{11}\ L_\odot \lesssim L_{IR} \lesssim 8.7\times10^{12}\ L_\odot$. Among the 21 galaxies analyzed here, as many as 8 have IR luminosities comparable to Ultra-Luminous InfraRed Galaxies[15] (ULIRGs, i.e. $L_{IR} > 10^{12}\ L_\odot$, see Lonsdale et al. 2006). This finding is quite surprising as ALPINE galaxies are selected as UV-brightest sources in the given redshift range $z = 4-6$. Our results suggest that a large fraction of their star formation is dust-obscured, which is consistent with stacking results by Fudamoto et al. (2020) (suggesting that on average 45% of SFR is obscured at $z = 5-6$).

The inferred IR luminosities correspond to obscured SFRs in the range $SFR_{IR} \sim 17-878\ M_\odot$/yr (assuming the conversion factor given in Table 2). The largest value for $SFR_{IR} = 878\ M_\odot$/yr is found in the galaxy DC 873756, the least UV-bright galaxy among the FIR continuum detected ALPINE sources. Its UV magnitude ($M_{UV} = -20.9$) corresponds to a monochromatic luminosity at 1500 Å around $L_{UV} = 10^{10.7}\ L_\odot$, implying an anattenuated[16] $SFR_{UV} = 4\ M_\odot$/yr. Compared to its surprisingly large SFR_{IR}, this implies that more than 99%

[14] In Fig. 3 we show the M_d detection threshold for the REBELS program assuming a non-detection flux limit of 42 μJy Inami et al. 2022 and the average dust temperature $T_d = 47\ \pm 7$ K.

[15] For comparison, only one ULIRG-like galaxy, REBELS-25, is found among the 13 REBELS galaxies (Sommovigo et al. 2022; Inami et al. 2022, see also Algera in prep. for a detailed analysis of the source).

[16] $SFR_{UV} = L_{UV}/\mathcal{K}_{1500}$, where the conversion coefficient $\mathcal{K}_{1500} = 1.174\times10^{10}\ L_\odot/(M_\odot yr^{-1})$ is taken from Ferrara et al. (2022).

of the SFR in DC 873756 is obscured[17]. These results is highly in contrast with UV-to-optical SED-fitting results by Faisst et al. (2020a), who derive a total, dust-corrected $\mathrm{SFR_{SED}} = 5^{+10}_{-2}$ $\mathrm{M_\odot/yr}$. Using only UV-to-optical data the total SFR of DC 873756 was underestimated by more than two orders of magnitude[18].

In order to understand the nature of this discrepancy and whether DC 873756 represents an isolated case, in Fig. 4 we compare the SFR derived from UV-to-optical SED-fitting with $\mathrm{SFR_{UV}} + \mathrm{SFR_{IR}}$ for all the ALPINE sources considered here. We find that in most cases (80%) the two methods give consistent results within $1-\sigma$. The uncertainties on $\mathrm{SFR_{IR}}$ are very large (see Tab. 2) due to the strong dependence of this quantity on T_d ($\mathrm{SFR_{IR}} \propto L_\mathrm{IR} \propto T_\mathrm{d}^6$), which is only constrained within ±10 K. There are 4 outliers (DC 539609, VC 5100969402, DC 873756, VC 5101218326); for these sources the ratio[19] between the UV-to-optical SED-derived SFR and that obtained from our method is $< 1/3$. In all these sources strong FIR continuum emission ($\mathrm{SFR_{IR}} > 100$ $\mathrm{M_\odot/yr}$) coexists with blue UV slopes $\beta_\mathrm{UV} < -1$, which would in contrast suggest low dust obscuration. These 4 galaxies are highlighted in Fig. 4, with the two most extreme cases being the galaxies DC 873756 and VC 5101218326. We note that if we do not include these two sources in the $\mathrm{SFR_{SED}}$ vs. $\mathrm{SFR_{UV}} + \mathrm{SFR_{IR}}$ linear fit we recover a slope which is perfectly consistent with the bisector 1.1 ± 0.4 (albeit the large scatter), whereas if we include them we find -0.1 ± 0.1.

One possible scenario to explain these peculiar galaxies is that they host Active Galactic Nuclei (AGN). Indeed, (Di Mascia & al., in prep. 2022) show that AGN can emit significantly not only at MIR, but also at FIR wavelengths. Thus, not accounting for AGN contribution, results in an overestimation of the host galaxy L_IR and obscured $\mathrm{SFR_{IR}}$. However, this scenario seems unlikely based on these ALPINE galaxies optical-to-UV spectra, which do not show any peculiar feature with respect to the other sources in the sample. Nevertheless, whether AGN could contribute to the FIR emission of the most massive ALPINE galaxies such as VC 5101218326 (whose $M_\star = 10^{11}$ $\mathrm{M_\odot}$ is the largest among all ALPINE galaxies) is still an open question (Barchiesi et al. in prep., Shen at al. in prep, Faisst et al. 2022).

A clue for the interpretation of these outliers comes from computing their molecular index (Ferrara et al. 2022):

$$I_\mathrm{m} = \frac{(F_{1900}/F_\mathrm{UV})}{(\beta_\mathrm{UV} - \beta_\mathrm{int})} \tag{8}$$

where $\beta_\mathrm{int} = -2.406$ for the MW. Assuming the interstellar medium (ISM) to be described by a single zone model, where dust and stars are uniformly mixed[20], Ferrara et al. (2022) obtains the following analytical expression for $I_\mathrm{m} \sim 7062\ xe^{-3x^{1/6}}$, where $x = Zt_\mathrm{dep}/(\beta - \beta_\mathrm{int})$. This expression has a maximum $I_\mathrm{m}^* \simeq 1120$ (located at $x = 64$). Indeed, F_{1900} and thus I_m can be increased by raising either the dust mass or the temperature. However, increasing T_d requires larger effective optical depths ($\beta_\mathrm{UV} - \beta_\mathrm{int}$) (see also Sec. 3.1), which are excluded in a relatively transparent single zone medium. It is possible to raise M_d while keeping ($\beta_\mathrm{UV} - \beta_\mathrm{UV,int}$) low, but this implies pushing the dust temperatures progressively closer to T_CMB, thus preventing F_{1900}, and hence I_m, to increase indefinitely. Interestingly, we find that the only galaxies in the ALPINE sample for which $I_\mathrm{m} > I_\mathrm{m}^*$ are the outliers in Fig. 4 (see also Tab. 2 for the I_m value of each source), with the largest value $I_\mathrm{m} = 6752$ corresponding to the most peculiar galaxy DC 873756.

These large I_m values[21] can be achieved only if the FIR and UV emitting regions are spatially decoupled (Ferrara et al. 2022). In this scenario, the observed strong FIR continuum emission in these peculiar ALPINE galaxies comes from optically thick, star-forming clumps (likely, giant molecular complexes), whereas the small UV optical depth (i.e. blue β_UV) traces the diffuse, interclump gas component in which young stars are embedded after they disperse their natal cloud (see also Faisst et al. 2017). This scenario, referred to as "spatial-segregation" of UV and IR emission has been proposed by other theoretical works focusing on sources at the EoR (Behrens et al. 2018; Liang et al. 2019; Sommovigo et al. 2020; Pallottini et al. 2022; Dayal et al. 2022). Current ALMA observations do not to probe the ISM morphology down to such scales ($\ll 1$ kpc). Future ALMA observations at higher spatial resolution, combined with JWST images (see e.g. $\propto 100$ pc resolution images of $z = 6-8$ galaxies by Chen et al. 2022a) will help us confirm or discard the scenario proposed here.

So far, a significant spatial offset between ALMA and HST data has been observed in some $z > 5$ star-forming galaxies (Hodge et al. 2012; Carniani et al. 2017; Laporte et al. 2017; Inami et al. 2022; Bowler et al. 2018). At lower redshift, spatial-segregation has been invoked to motivate the blue β_UV slopes found in some $z \sim 2$ dusty star forming galaxies (DSFGs, Casey et al. 2014), which strongly deviate from the local IRX-β relation (where $\mathrm{IRX} = L_\mathrm{FIR}/L_\mathrm{UV}$). Similarly, the IRX excess observed in some $z \sim 2$ starbursts (Elbaz et al. 2018) and $z \sim 4.5$ sub-mm galaxies (Gómez-Guijarro et al. 2018) has been associated to spatially decoupled UV and IR emission in resolved ALMA and HST maps.

6 SUMMARY

In this paper, we study the dust continuum emission properties of the Far Infrared (FIR) continuum detected $z = 5$ galaxies from the ALMA Large Program ALPINE (Le Fèvre et al. 2020; Faisst et al. 2020a). To derive their dust temperature T_d using the single available FIR continuum observation (at rest-frame 158 μm), we apply the method presented in

[17] Following the same procedure, we infer obscured SFR fractions in the range $\sim 60-90\%$ for the remaining ALPINE galaxies.
[18] We note that a milder correction to account for the obscured SFR fraction was already applied by Schaerer et al. (2020) to some ALPINE galaxies; due to the lack of constraints on individual galaxies IR luminosities, they relied on the dust temperature derived by Béthermin et al. (2020) from stacking.
[19] This discrepancy is larger than what can be explained by the different assumptions on the IMF in the two derivations (here we assume a Salpeter $1-100$ $\mathrm{M_\odot}$, whereas Faisst et al. 2020a adopt a Chabrier.
[20] And UV and IR emission are co-spatial
[21] $I_\mathrm{m} > I_\mathrm{m}^*$ are also measured in few REBELS galaxies (4 out of the 14 continuum detected sources)

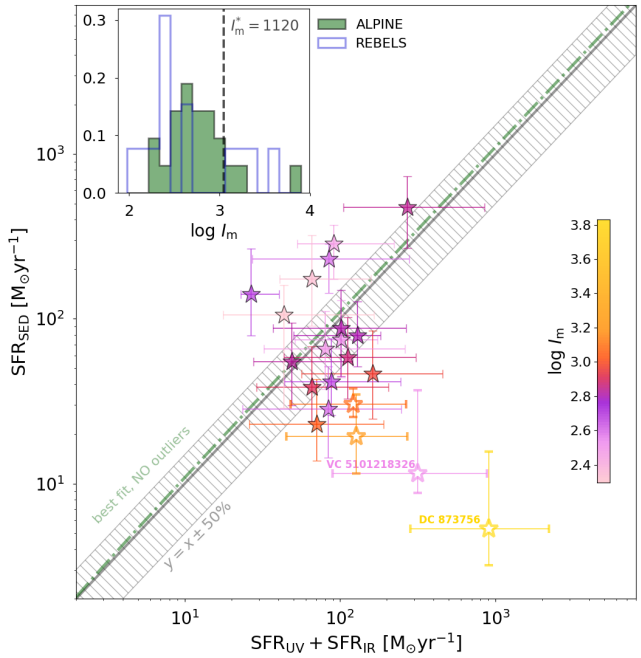

Figure 4. Main panel: Total SFR inferred for ALPINE galaxies through dust-corrected optical-to-UV SED fitting, SFR$_{SED}$ (Faisst et al. 2020a) vs. that obtained from the UV and IR luminosities multiplied by the corresponding calibration factors, SFR$_{UV}$ + SFR$_{IR}$. The dashed area shows the area around the bisector ±50% uncertainty. The light green symbols represent the most peculiar sources in the sample, for which SFR$_{IR}$ > 100 M$_\odot$/yr, largely deviating from the SFR deduced from optical-to-UV data SFR$_{SED}$ < 30 M$_\odot$/yr. The green dotted dashed line shows slope of the best fitting linear relation obtained when excluding these outliers, consistent with the bisector. **Inset panel:** Distribution of the molecular index $I_m = (F_{1900}/F_{UV})/(\beta_{UV} - \beta_{int})$ among the ALPINE continuum detected galaxies. The vertical dashed line shows the upper limit $I_m^* = 1120$ obtained in a single phase ISM model, where UV and IR emission are cospatial. This limit is exceeded in 3 among the 21 ALPINE galaxies considered here, which correspond to the outliers in the main plot (but one). We speculate that these peculiar galaxies have spatially segregated UV and IR emission.

Sommovigo et al. (2021). This method relies on the combination of the dust continuum flux with the overlying [C II] emission line luminosity; L_{CII} serves as a proxy for the dust mass M_d, breaking the degeneracy between M_d and T_d in the FIR SED fitting procedure.

Having constrained T_d and M_d for all the ALPINE galaxies, we can uniquely derive dust-temperature-dependent properties such as the IR luminosity L_{IR} and obscured SFR fraction SFR$_{IR}$. Providing this insight for ALPINE galaxies is fundamental as they constitute the most abundant sample of dusty star-forming galaxies at $z > 4$. Moreover, using the results from Sommovigo et al. (2022), we can compare them with the higher-z REBELS galaxies (Bouwens et al. 2022), consistently investigating the cosmic evolution of dust properties in an unprecedentedly large number of sources from $z \sim 5$ to $z \sim 7$.

We summarize below our findings:

- The dust temperatures for ALPINE galaxies vary within the range 25 − 60 K. The average value $\langle T_d \rangle = 48 \pm 8$ K is consistent with the result from stacked SED fitting by Béthermin et al. (2020). It also matches the predictions from the physical model for the cosmic T_d evolution by Sommovigo et al. (2022), which finds a mild increase in the dust temperature with redshift $T_d \propto (1+z)^{0.4}$;
- Dust masses for ALPINE galaxies are in the $0.6-25.1 \times 10^7$ M$_\odot$ range. Due to the ∼ 2 times warmer T_d that we infer for ALPINE galaxies, M_d are 7 times lower than previously reported by Pozzi et al. (2021). Thus, the resulting dust yields $\langle M_d/M_\star \rangle = 2\times10^{-3}$ are now consistent with theoretical dust production constraints at $z \sim 5$. In particular, we do not need to invoke extreme scenarios, e.g. saturated grain growth or no dust destruction, which might instead be needed at $z \sim 7$ for a few peculiar REBELS galaxies (see also Dayal et al. 2022).
- The linear $M_d - M_\star$ relation predicted by theoretical models is consistent with our results, differently from what is found at $z \sim 7$ for REBELS galaxies where it appears flat. This might be evidence of a rapid evolution of the $M_d - M_\star$ relation at $z > 5$. However, probing a wider stellar mass range at both redshifts is needed to completely exclude that this is due to an observational bias;
- We find 8 ALPINE sources with $L_{IR} > 10^{12}$ L$_\odot$, comparable to Ultra-Luminous InfraRed Galaxies (ULIRGs). Among these 8 ULIRGs-like sources, there are 4 extreme systems where SFR$_{IR}$ > 100 M$_\odot$/yr, exceeding by a factor > 3 the total SFR deduced from UV-to-optical SED fitting. These outliers are the only sources showing large molecular index values $I_m = (F_{1900}/F_{UV})/(\beta_{UV} - \beta_{int}) > 1120$, the critical value for a single phase ISM (Ferrara et al. 2022). We thus predict that these outliers are spatially-segregated systems, where FIR emission comes from clumpy giant molecular clouds whereas the UV arises from the diffuse, UV transparent ISM.

High-resolution observations at sub-kpc scales for both the UV (such as Chen et al. 2022a) and the dust continuum (also including shorter-wavelengths ALMA bands 8 and 9) of the ALPINE spatially-segregated galaxies will help us clarify the morphology of their ISM. An immediate improvement will be provided by upcoming high-resolution ALMA band 6 observations within the CRISTAL large program (PI: Herrera-Camus) and by JWST, whose pointings include 2 of these 4 peculiar sources.

ACKNOWLEDGEMENTS

AF, AP, LS, SC acknowledge support from the ERC Advanced Grant INTERSTELLAR H2020/740120 (PI: Ferrara). Any dissemination of results must indicate that it reflects only the author's view and that the Commission is not responsible for any use that may be made of the information it contains. Partial support from the Carl Friedrich von Siemens-Forschungspreis der Alexander von Humboldt-Stiftung Research Award is kindly acknowledged (AF). PD acknowledges support from the ERC starting grant DELPHI StG-717001, from the NWO grant ODIN 016.VIDI.189.162 and the European Commission's and University of Groningen's CO-FUND Rosalind Franklin program.

Table 1. Measured properties of the 21 [C II] and continuum detected ALPINE galaxies together with adopted relative errors ($[z, L_{\rm CII}, F_{1900}]$ from Béthermin et al. 2020, $[M_\star, M_{\rm UV}, \beta_{\rm UV}]$ from Faisst et al. 2020a, and $[r_{\rm CII}, r_\star]$ from Fujimoto et al. 2020). The value of $r_{\rm CII}$ derived in this work is marked with a * (see Sec. 2 for the details). We also show the molecular index value $I_{\rm m}$ (see eq. 8) directly derived from the data.

[C II] AND CONTINUUM DETECTED ALPINE GALAXIES: DATA									
name	z	$L_{\rm CII}$	F_{1900}	$\log M_\star$	$r_{\rm CII}$	$r_\star$	$M_{\rm UV}$	$\beta_{\rm UV}$	$I_{\rm m}$
		[10^8 L$_\odot$]	[μJy]	[M$_\odot$]	[kpc]	[kpc]	[mag]		
CG 32	4.4105	8.2 ± 0.8	230 ± 65	$9.75^{+0.24}_{-0.29}$	1.94 ± 0.3	0.91 ± 0.13	−21.274	−0.859157	397
DC 396844	4.5424	11.5 ± 1.0	346 ± 69	$9.86^{+0.14}_{-0.19}$	2.56 ± 0.33	0.58 ± 0.2	−21.665	−1.38062	658
DC 417567	5.6700	3.1 ± 0.5	201 ± 60	$9.81^{+0.18}_{-0.11}$	2.07 ± 0.58	0.65 ± 0.20	−22.919	−1.86659	320
DC 422677	4.4381	4.2 ± 0.7	375 ± 123	$9.85^{+0.14}_{-0.16}$	1.10 ± 0.50	0.58 ± 0.14	−21.634	−1.2423	624
DC 488399	5.6704	10.8 ± 0.5	252 ± 32	$10.20^{+0.13}_{-0.15}$	1.32 ± 0.16	0.47 ± 0.32	−22.058	−1.88283	913
DC 493583	4.5134	4.3 ± 0.6	235 ± 81	$9.61^{+0.15}_{-0.11}$	1.89 ± 0.51	0.64 ± 0.17	−21.765	−2.01243	1051
DC 494057(HZ4)	5.5448	7.2 ± 0.5	179 ± 30	$10.15^{+0.13}_{-0.15}$	2.48 ± 0.25	0.88 ± 0.16	−22.373	−1.87832	466
DC 539609	5.1818	4.9 ± 0.6	187 ± 54	$9.38^{+0.12}_{-0.12}$	1.65 ± 0.43	0.77 ± 0.16	−22.357	−2.20637	1179
DC 683613	5.5420	7.8 ± 0.7	245 ± 54	$10.17^{+0.14}_{-0.15}$	1.82 ± 0.33	0.57 ± 0.24	−21.428	−1.3048	729
DC 848185(HZ6)	5.2931	16.0 ± 0.95	319 ± 50	$10.37^{+0.08}_{-0.19}$	3.47 ± 0.25	0.9 ± 0.3	−22.54	−1.14217	277
DC 881725	4.5777	6.87 ± 0.63	349 ± 90	$9.96^{+0.16}_{-0.11}$	2.26 ± 0.33	0.67 ± 0.21	−21.553	−1.20243	634
VC 5100822662	4.5205	7.86 ± 0.65	210 ± 38	$10.17^{+0.13}_{-0.14}$	2.59 ± 0.37	1.32 ± 0.33	−21.891	−1.31549	303
VC 5100969402	4.5785	5.23 ± 0.55	327 ± 99	$10.00^{+0.12}_{-0.14}$	1.62 ± 0.33	0.59 ± 0.15	−21.53	−1.94423	1583
VC 5100994794	4.5802	5.57 ± 0.51	117 ± 36	$9.73^{+0.15}_{-0.13}$	1.86 ± 0.32	1.63 ± 0.35	−21.342	−1.62524	398
VC 5101209780	4.5701	7.31 ± 1.56	311 ± 112	$10.05^{+0.12}_{-0.12}$	$3.25 \pm 0.72^*$	1.00 ± 0.24	−22.143	−1.91506	803
VE 530029038	4.4298	6.9 ± 0.8	125 ± 58	$9.93^{+0.21}_{-0.12}$	2.76 ± 0.65	1.96 ± 0.14	−21.95	−1.4904	197
DC 552206	5.5016	15.2 ± 1.1	285 ± 73	$10.58^{+0.14}_{-0.16}$	3.41 ± 0.35	0.96 ± 0.64	−22.642	−0.977538	211
DC 818760	4.5613	43.0 ± 1.7	1077 ± 130	$10.63^{+0.11}_{-0.10}$	2.59 ± 0.16	0.75 ± 0.17	−22.225	−0.548038	679
DC 873756	4.5457	36.2 ± 1.3	1354 ± 76	$10.25^{+0.08}_{-0.10}$	2.36 ± 0.11	1.08 ± 0.43	−20.869	−1.59125	6752
VC 5101218326	4.5739	18.3 ± 0.8	462 ± 79	$11.01^{+0.07}_{-0.05}$	2.37 ± 0.15	1.46 ± 0.32	−22.345	−0.86014	315
VC 5180966608	4.5296	13.7 ± 1.1	419 ± 84	$10.82^{+0.12}_{-0.13}$	5.10 ± 0.42	0.59 ± 0.24	−21.743	−0.826991	479

DATA AVAILABILITY

Data generated in this research will be shared on reasonable request to the corresponding author.

REFERENCES

Bakx T. J. L. C., et al., 2020, MNRAS, 493, 4294
Bakx T. J. L. C., et al., 2021, MNRAS, 508, L58
Barisic I., et al., 2017, ApJ, 845, 41
Behrens C., Pallottini A., Ferrara A., Gallerani S., Vallini L., 2018, MNRAS, 477, 552
Behroozi P., Wechsler R. H., Hearin A. P., Conroy C., 2019, MNRAS, 488, 3143
Béthermin M., et al., 2015, A&A, 573, A113
Béthermin M., et al., 2020, A&A, 643, A2
Bocchio M., Marassi S., Schneider R., Bianchi S., Limongi M., Chieffi A., 2016, A&A, 587, A157
Bouwens R. J., et al., 2016, ApJ, 833, 72
Bouwens R., et al., 2020, ApJ, 902, 112
Bouwens R. J., et al., 2022, ApJ, 931, 160
Bowler R. A. A., Bourne N., Dunlop J. S., McLure R. J., McLeod D. J., 2018, MNRAS, 481, 1631
Burgarella D., Nanni A., Hirashita H., Theulé P., Inoue A. K., Takeuchi T. T., 2020, A&A, 637, A32
Calzetti D., Armus L., Bohlin R. C., Kinney A. L., Koornneef J., Storchi-Bergmann T., 2000, ApJ, 533, 682
Capak P. L., et al., 2015, Nature, 522, 455
Carniani S., et al., 2017, A&A, 605, A42
Carniani S., et al., 2018a, MNRAS, 478, 1170
Carniani S., Maiolino R., Smit R., Amorín R., 2018b, ApJL, 854, L7
Carniani S., et al., 2020, MNRAS, 499, 5136
Casey C. M., et al., 2014, ApJ, 796, 95
Castellano M., et al., 2022, arXiv e-prints, p. arXiv:2207.09436
Chapman S. C., Blain A. W., Smail I., Ivison R. J., 2005, ApJ, 622, 772
Chen Z., Stark D. P., Endsley R., Topping M., Whitler L., Charlot S., 2022a, arXiv e-prints, p. arXiv:2207.12657
Chen Y. Y., Hirashita H., Wang W.-H., Nakai N., 2022b, MNRAS, 509, 2258
Chevallard J., et al., 2019, MNRAS, 483, 2621
Clements D. L., et al., 2018, MNRAS, 475, 2097
Correa C. A., Wyithe J. S. B., Schaye J., Duffy A. R., 2015, MNRAS, 450, 1521
Curti M., et al., 2022, arXiv e-prints, p. arXiv:2207.12375
Daddi E., et al., 2010, ApJL, 714, L118
Dayal P., Ferrara A., Dunlop J. S., Pacucci F., 2014, MNRAS, 445, 2545
Dayal P., et al., 2022, MNRAS, 512, 989
De Breuck C., et al., 2019, A&A, 631, A167
De Looze I., et al., 2014, A&A, 568, A62

Table 2. Predicted properties of the 21 [C II] and continuum detected ALPINE galaxies, respectively: [C II]-to-total gas conversion factor $\alpha_{\rm CII}$ (eq. 5), dust temperature $T_{\rm d}$ and mass $M_{\rm d}$, IR luminosity $\log L_{\rm IR}$, SN dust yield y_d and obscured SFR, $\rm SFR_{IR}[M_\odot yr^{-1}] = 10^{-10}\ L_{IR}[L_\odot]$ (Kennicutt 1998).

[C II] AND CONTINUUM DETECTED ALPINE GALAXIES: RESULTS						
name	$\alpha_{\rm CII}$	$T_{\rm d}$	$\log M_{\rm d}$	$y_{\rm d}$	$\log L_{\rm IR}$	$\rm SFR_{IR}$
		[K]	[$M_\odot$]	[$M_\odot$/SN]	[$L_\odot$]	[$M_\odot$/yr]
CG 32	4^{+5}_{-2}	51^{+18}_{-15}	$7.20^{+0.34}_{-0.25}$	$0.15^{+0.18}_{-0.07}$	$11.87^{+0.54}_{-0.56}$	75^{+182}_{-54}
DC 396844	12^{+11}_{-5}	37^{+12}_{-8}	$7.75^{+0.31}_{-0.29}$	$0.41^{+0.43}_{-0.2}$	$11.6^{+0.45}_{-0.33}$	40^{+73}_{-21}
DC 417567	16^{+19}_{-6}	48^{+11}_{-13}	$7.33^{+0.33}_{-0.24}$	$0.18^{+0.2}_{-0.08}$	$11.9^{+0.29}_{-0.46}$	79^{+75}_{-51}
DC 422677	9^{+11}_{-5}	54^{+11}_{-14}	$7.24^{+0.32}_{-0.33}$	$0.13^{+0.14}_{-0.07}$	$12.11^{+0.16}_{-0.47}$	128^{+58}_{-84}
DC 488399	5^{+6}_{-2}	53^{+16}_{-15}	$7.38^{+0.34}_{-0.22}$	$0.08^{+0.1}_{-0.03}$	$12.2^{+0.47}_{-0.5}$	157^{+308}_{-108}
DC 493583	10^{+11}_{-4}	48^{+15}_{-14}	$7.25^{+0.33}_{-0.24}$	$0.23^{+0.26}_{-0.1}$	$11.79^{+0.45}_{-0.54}$	61^{+111}_{-44}
DC 494057 **(HZ4)**	8^{+9}_{-3}	47^{+16}_{-12}	$7.37^{+0.35}_{-0.26}$	$0.09^{+0.11}_{-0.04}$	$11.83^{+0.5}_{-0.45}$	68^{+145}_{-44}
DC 539609	6^{+7}_{-2}	55^{+14}_{-15}	$7.13^{+0.31}_{-0.22}$	$0.30^{+0.31}_{-0.12}$	$12.0^{+0.36}_{-0.53}$	101^{+132}_{-71}
DC 683613	8^{+10}_{-3}	49^{+15}_{-13}	$7.43^{+0.35}_{-0.24}$	$0.10^{+0.12}_{-0.04}$	$12.01^{+0.48}_{-0.48}$	102^{+206}_{-68}
DC 848185 **(HZ6)**	11^{+13}_{-5}	39^{+13}_{-9}	$7.86^{+0.36}_{-0.3}$	$0.16^{+0.21}_{-0.08}$	$11.86^{+0.48}_{-0.34}$	73^{+145}_{-40}
DC 881725	11^{+12}_{-4}	47^{+14}_{-13}	$7.49^{+0.34}_{-0.24}$	$0.18^{+0.22}_{-0.08}$	$11.96^{+0.46}_{-0.49}$	91^{+172}_{-62}
VC 5100822662	5^{+5}_{-2}	50^{+18}_{-14}	$7.2^{+0.35}_{-0.25}$	$0.06^{+0.07}_{-0.02}$	$11.86^{+0.54}_{-0.52}$	72^{+178}_{-51}
VC 5100969402	9^{+11}_{-4}	52^{+13}_{-14}	$7.33^{+0.32}_{-0.24}$	$0.11^{+0.13}_{-0.05}$	$12.06^{+0.33}_{-0.53}$	116^{+133}_{-81}
VC 5100994794	2^{+3}_{-1}	60^{+19}_{-19}	$6.77^{+0.34}_{-0.23}$	$0.06^{+0.07}_{-0.02}$	$11.87^{+0.48}_{-0.64}$	75^{+153}_{-58}
VC 5101209780	11^{+13}_{-4}	42^{+16}_{-12}	$7.53^{+0.35}_{-0.28}$	$0.16^{+0.2}_{-0.08}$	$11.72^{+0.55}_{-0.5}$	52^{+135}_{-36}
VE 530029038	3^{+4}_{-1}	48^{+21}_{-16}	$6.97^{+0.35}_{-0.27}$	$0.06^{+0.07}_{-0.03}$	$11.5^{+0.66}_{-0.69}$	31^{+113}_{-25}
DC 552206	10^{+12}_{-4}	37^{+13}_{-9}	$7.79^{+0.37}_{-0.3}$	$0.09^{+0.12}_{-0.04}$	$11.66^{+0.48}_{-0.34}$	45^{+93}_{-25}
DC 818760	6^{+7}_{-2}	45^{+16}_{-12}	$8.04^{+0.36}_{-0.28}$	$0.14^{+0.17}_{-0.06}$	$12.38^{+0.53}_{-0.45}$	240^{+575}_{-154}
DC 873756	5^{+5}_{-1}	59^{+14}_{-16}	$7.88^{+0.32}_{-0.17}$	$0.22^{+0.24}_{-0.07}$	$12.94^{+0.38}_{-0.55}$	878^{+1233}_{-628}
VC 5101218326	3^{+3}_{-1}	59^{+17}_{-18}	$7.40^{+0.34}_{-0.2}$	$0.01^{+0.02}_{-0.0}$	$12.48^{+0.46}_{-0.59}$	303^{+569}_{-225}
VC 5180966608	47^{+54}_{-21}	25^{+6}_{-4}	$8.41^{+0.35}_{-0.31}$	$0.20^{+0.26}_{-0.1}$	$11.23^{+0.22}_{-0.12}$	17^{+11}_{-4}

Dekel A., Krumholz M. R., 2013, MNRAS, 432, 455
Dessauges-Zavadsky M., et al., 2020, A&A, 643, A5
Di Mascia F., al., in prep. 2022, 0, 0
Draine B. T., 1989, in Böhm-Vitense E., ed., Infrared Spectroscopy in Astronomy. p. 93
Draine B. T., 2003, ARA&A, 41, 241
Draine B. T., Li A., 2007, ApJ, 657, 810
Elbaz D., et al., 2018, A&A, 616, A110
Faisst A. L., et al., 2017, ApJ, 847, 21
Faisst A. L., et al., 2020a, ApJS, 247, 61
Faisst A. L., Fudamoto Y., Oesch P. A., Scoville N., Riechers D. A., Pavesi R., Capak P., 2020b, MNRAS, 498, 4192
Faisst A. L., et al., 2022, arXiv e-prints, p. arXiv:2206.03510
Fakhouri O., Ma C.-P., Boylan-Kolchin M., 2010, MNRAS, 406, 2267
Ferrara A., Tolstoy E., 2000, MNRAS, 313, 291
Ferrara A., Vallini L., Pallottini A., Gallerani S., Carniani S., Kohandel M., Decataldo D., Behrens C., 2019, MNRAS, 489, 1
Ferrara A., et al., 2022, MNRAS, 512, 58
Fudamoto Y., et al., 2020, A&A, 643, A4
Fujimoto S., et al., 2019, ApJ, 887, 107
Fujimoto S., et al., 2020, ApJ, 900, 1
Galliano F., Dwek E., Chanial P., 2008, ApJ, 672, 214
Ginolfi M., et al., 2020, A&A, 633, A90
Gómez-Guijarro C., et al., 2018, ApJ, 856, 121
Harikane Y., et al., 2020, ApJ, 896, 93
Hashimoto T., et al., 2019, Pub. Astron. Soc. Japan, 71, 71
Hodge J. A., Carilli C. L., Walter F., de Blok W. J. G., Riechers D., Daddi E., Lentati L., 2012, ApJ, 760, 11
Huang J. S., et al., 2014, ApJ, 784, 52
Inami H., et al., 2022, MNRAS,
James A., Dunne L., Eales S., Edmunds M. G., 2002, MNRAS, 335, 753
Jones T., Sanders R., Roberts-Borsani G., Ellis R. S., Laporte N., Treu T., Harikane Y., 2020, ApJ, 903, 150
Kennicutt Robert C. J., 1998, ApJ, 498, 541
Labbe I., et al., 2022, arXiv e-prints, p. arXiv:2207.12446
Laporte N., et al., 2017, ApJL, 837, L21
Laporte N., et al., 2019, MNRAS, 487, L81
Le Fèvre O., et al., 2020, A&A, 643, A1
Leitherer C., et al., 1999, ApJS, 123, 3
Leroy A. K., et al., 2011, ApJ, 737, 12
Leśniewska A., Michałowski M. J., 2019, A&A, 624, L13
Liang L., et al., 2019, MNRAS, p. 2072
Liu H.-M., Hirashita H., 2019, MNRAS, 490, 540
Lonsdale C. J., Farrah D., Smith H. E., 2006, Ultraluminous Infrared Galaxies. Springer Berlin Heidelberg, p. 285, doi:10.1007/3-540-30313-8_9
Ma X., Hopkins P. F., Faucher-Giguère C.-A., Zolman N., Muratov A. L., Kereš D., Quataert E., 2016, MNRAS, 456, 2140
Magdis G. E., et al., 2012, ApJ, 760, 6
Magdis G. E., et al., 2014, ApJ, 796, 63
Magnelli B., et al., 2013, A&A, 553, A132
Magnelli B., et al., 2014, A&A, 561, A86
Maiolino R., Mannucci F., 2019, A&A Rev., 27, 3

Mancini M., Schneider R., Graziani L., Valiante R., Dayal P., Maio U., Ciardi B., Hunt L. K., 2015, MNRAS, 451, L70
Matsuura M., et al., 2019a, MNRAS, 482, 1715
Matsuura M., et al., 2019b, Astro2020: Decadal Survey on Astronomy and Astrophysics, 2020, 573
Matthee J., et al., 2017, ApJ, 851, 145
Matthee J., et al., 2019, ApJ, 881, 124
Meurer G. R., Heckman T. M., Calzetti D., 1999, ApJ, 521, 64
Naidu R. P., et al., 2022, arXiv e-prints, p. arXiv:2207.09434
Nanni A., Burgarella D., Theulé P., Côté B., Hirashita H., 2020, A&A, 641, A168
Pallottini A., et al., 2019, MNRAS, 487, 1689
Pallottini A., et al., 2022, MNRAS, 513, 5621
Pereira-Santaella M., Rigopoulou D., Farrah D., Lebouteiller V., Li J., 2017, MNRAS, 470, 1218
Planck Collaboration et al., 2016, A&A, 596, A107
Popping G., Somerville R. S., Galametz M., 2017, MNRAS, 471, 3152
Pozzi F., et al., 2021, A&A, 653, A84
Rémy-Ruyer A., et al., 2014, A&A, 563, A31
Reuter C., et al., 2020, ApJ, 902, 78
Romano M., et al., 2021, A&A, 653, A111
Rowlands K., Gomez H. L., Dunne L., Aragón-Salamanca A., Dye S., Maddox S., da Cunha E., van der Werf P., 2014, MNRAS, 441, 1040
Rybak M., et al., 2019, ApJ, 876, 112
Schaerer D., et al., 2020, A&A, 643, A3
Schreiber C., Elbaz D., Pannella M., Ciesla L., Wang T., Franco M., 2018, A&A, 609, A30
Slavin J. D., Dwek E., Mac Low M.-M., Hill A. S., 2020a, ApJ, 902, 135
Slavin J. D., Dwek E., Mac Low M.-M., Hill A. S., 2020b, ApJ, 902, 135
Sommovigo L., Ferrara A., Pallottini A., Carniani S., Gallerani S., Decataldo D., 2020, MNRAS, 497, 956
Sommovigo L., Ferrara A., Carniani S., Zanella A., Pallottini A., Gallerani S., Vallini L., 2021, MNRAS, 503, 4878
Sommovigo L., et al., 2022, MNRAS, 513, 3122
Song M., et al., 2016, ApJ, 825, 5
Tacconi L. J., Genzel R., Sternberg A., 2020, ARA&A, 58, 157
Tamura Y., et al., 2019, ApJ, 874, 27
Todini P., Ferrara A., 2001, MNRAS, 325, 726
Topping M. W., et al., 2022, MNRAS, 516, 975
Torrey P., et al., 2019, MNRAS, 484, 5587
Triani D. P., Sinha M., Croton D. J., Pacifici C., Dwek E., 2020, MNRAS, 493, 2490
Ucci G., et al., 2021, arXiv e-prints, p. arXiv:2112.02115
Vallini L., Ferrara A., Pallottini A., Carniani S., Gallerani S., 2020, MNRAS, 495, L22
Vallini L., Ferrara A., Pallottini A., Carniani S., Gallerani S., 2021, MNRAS, 505, 5543
Vanderhoof B. N., et al., 2022, MNRAS, 511, 1303
Viero M. P., et al., 2013, ApJ, 779, 32
Viero M. P., Sun G., Chung D. T., Moncelsi L., Condon S. S., 2022, MNRAS, 516, L30
Vijayan A. P., Clay S. J., Thomas P. A., Yates R. M., Wilkins S. M., Henriques B. M., 2019, MNRAS, 489, 4072
Walter F., et al., 2020, ApJ, 902, 111
Weaver J. R., et al., 2022, ApJS, 258, 11
Weingartner J. C., Draine B. T., 2001, ApJ, 548, 296
Witstok J., et al., 2022, MNRAS, 515, 1751
Yang M., Greve T. R., Dowell C. D., Borys C., 2007, ApJ, 660, 1198
Zanella A., et al., 2018, MNRAS, 481, 1976